Mesoporous MgO promoted with $NaNO_3/NaNO_2$ for rapid and high-capacity CO_2 capture at moderate temperatures

Xiao Zhao, Guozhao Ji, Wen Liu, Xu He, Edward J. Anthony, Ming Zhao

PII: S1385-8947(17)31567-X
DOI: http://dx.doi.org/10.1016/j.cej.2017.09.068
Reference: CEJ 17653

To appear in: *Chemical Engineering Journal*

Received Date: 7 July 2017
Revised Date: 8 September 2017
Accepted Date: 9 September 2017

Please cite this article as: X. Zhao, G. Ji, W. Liu, X. He, E.J. Anthony, M. Zhao, Mesoporous MgO promoted with $NaNO_3/NaNO_2$ for rapid and high-capacity CO_2 capture at moderate temperatures, *Chemical Engineering Journal* (2017), doi: http://dx.doi.org/10.1016/j.cej.2017.09.068

Chemical Engineering Journal, Vol. 332, 15 January 2018, pp. 216-226
DOI:10.1016/j.cej.2017.09.068

Mesoporous MgO promoted with $NaNO_3/NaNO_2$ for rapid and high-capacity CO_2 capture at moderate temperatures

Xiao Zhao[a], Guozhao Ji[a], Wen Liu[b], Xu He[a], Edward J. Anthony[c], Ming Zhao[a,*]

[a] School of Environment, Tsinghua University, Beijing, 100084, China

[b] School of Civil and Environmental Engineering, Georgia Institute of Technology, Atlanta, GA 30332, USA

[c] Cranfield University, Cranfield, Bedfordshire MK43 0AL, UK

*Corresponding author. Phone: +86 10 62784701; E-mail: ming.zhao@tsinghua.edu.cn

Abstract: A series of mesoporous MgO samples with different morphologies were synthesized through a simple hydrothermal treatment and $NaNO_3$/$NaNO_2$ were used as promoters to enhance CO_2 capture capacity at an intermediate temperature range (200-400 °C). The effects of hydrothermal solution pH and content of promoters were examined to determine the optimal synthesis conditions. The influence of operational temperatures, CO_2 partial pressure, and performance over repeated cycles was investigated and the reaction mechanism was discussed. The mesoporous MgO promoted by $NaNO_3$/$NaNO_2$ exhibited a CO_2 capture capacity as high as 19.8 mmol·g^{-1} at 350 °C in the presence of 0.85 bar of CO_2 within only 50 min. A "three-stage" reaction process was proposed based on a detailed sorption kinetics study, namely Stage I: initiating interactions between CO_2 and exposed MgO; Stage II: generation and accumulation of Mg^{2+} and CO_3^{2-}; and Stage III: fast carbonation. Gradual deterioration of sorbents was found over the first 5 cycles followed by stable regenerability in the 5-15th cycles. A kinetic study of the 15th cycle suggests that the deactivation of sorbents inhibited the accumulation of Mg^{2+} and CO_3^{2-} in Stage II and suppressed the carbonation in Stage III. A range of characterizations were undertaken revealing the morphology and structure of both fresh and regenerated sorbents. The results confirmed that, other than the sintering effect due to phase transition, the transformation of MgO skeleton is also an important contributor to the gradual deactivation of the sorbents over the first 5 cycles. More severe sintering effect under harsh decarbonation conditions suppressed the stability of the sorbents over cycles.

Keywords: CO_2 capture, moderate-temperature sorbent, rapid absorption, mesoporous MgO, molten state promoters

1. Introduction

The increasing level of atmospheric CO_2 is a crucial challenge today, since CO_2 is widely accepted as the key greenhouse gas [1]. The application of carbon capture and storage (CCS) technology is considered a central strategy to stabilize the global CO_2 level [2]. So far, monoethanolamine (MEA) is the only commercialized CO_2 sorbent that is applied at temperatures lower than 200 °C [2,3]; nevertheless, this aqueous absorption technology suffers from a high energy penalty and capital costs, and is also challenged for environmental impacts [4,5]. High-temperature solid sorbents such as CaO have also been intensively studied in recent decades; however, the extremely high operational temperatures, i.e., sorption at ~ 650 °C and desorption at > 900 °C, causes severe sintering, and leads to increased complexity for heat integration design [6-9]. Development of intermediate-temperature (200-400 °C) solid sorbents are thus an emerging goal for research directed to find reliable, cost-effective CO_2 capture technologies [5].

As a potential candidate for intermediate-temperature CO_2 capture, MgO-based materials have attracted considerable research interest [5,10], owing to their high theoretical CO_2 capture capacity (1.09 g or 24.8 mmol of CO_2 per gram of MgO) and low regeneration energy (2.68 $kJ \cdot g^{-1}$ of CO_2) [11]. For comparison, in the case of the well-known high-capacity sorbent, CaO, 1 gram of CaO can carry CO_2 up to 0.79 g or 17.9 mmol in the case of complete carbonation. Additional advantages with MgO include high specific surface area and high pore volume [12-14]. The conversion of MgO to $MgCO_3$ is believed to be limited kinetically, rather than thermodynamically [15,16], and the intrinsically high lattice enthalpy restrains MgO from achieving a fast reaction with CO_2 [17]; moreover, the rigid carbonate "shell" would inhibit CO_2

molecules from accessing more deeply into the MgO structure [18]. These factors mean that MgO has an extremely low capacity of 0.24 mmol·g^{-1} at 200 °C using the unmodified material [15]. Thus, MgO is normally considered too poor a sorbent to be a feasible choice for CO_2 capture.

Commonly used strategies to improve the CO_2 capture capacity of MgO include enlarging the surface area [19-22], changing operation conditions [19,23,24], and incorporating promoters [25-29]. Among these strategies, the use of appropriate promoters has been proved to be most effective so far. Incorporation of K_2CO_3 into MgO sorbents through a precipitation method increased the CO_2 sorption capacity from ~0.2 to 1.9 mmol·g^{-1} at 375 °C and 1 bar of CO_2 [25]. A MgO·KNO_3 composite exhibits a maximum capacity of 3.2 mmol·g^{-1} at 325 °C in a pure CO_2 stream [27]. Zhang et al. synthesized a composite of MgO and $NaNO_3$ (80:20 by mass) via ball-milling, with the observation that the CO_2 sorption rate was greatly enhanced, leading to a maximum capacity of 15 mmol·g^{-1} at 375 °C and 1 bar of CO_2 [18]. A mesoporous MgO prepared using a supercritical drying process was found to be promoted by double sodium salts ($NaNO_3$ and Na_2CO_3) and exhibited a sorption capacity of 12.7 mmol·g^{-1} at 325 °C in a dry CO_2 stream and 11.5 mmol·g^{-1} at 275 °C in a wet CO_2 stream [14]. Use of multiple alkali metal nitrate/nitrite salts further improved both kinetics and capacity of CO_2 sorption for MgO (up to 15.7 mmol·g^{-1} at 340 °C) [29]. The melting point for $NaNO_3$ and $NaNO_2$ are 308 and 271 °C, respectively [30]. It has been concluded that alkali metal nitrates in molten/pre-molten state can serve as an effective phase transfer catalyst (PTC) promoting the gas-solid reaction between CO_2 and MgO [18]. A sorbent with higher capacity and faster kinetics is still highly probable, since the maximum MgO conversion in the open literature is < 85% [14,16,28,29,31]. Moreover, the role of each promoter in a double/triple promoting system needs to be investigated.

Alongside being used for post-combustion processes, MgO-based materials holds great potential for carbon capture in some pre-combustion processes, which requires intermediate to high temperature conditions. For example, in the Integrated Gasification Combined Cycle (IGCC) processes, the effluent gas from the shift reactors is at temperature ~ 250-400 °C with CO_2 concentration varying in range of 30-60 mol% [32]. It has been demonstrated that several MgO-based sorbents work efficiently in this temperature range [14,16,28,29,31]. However, the study on the effect of lower CO_2 partial pressure and wet conditions is still limited.

In this study, we synthesized a series of mesoporous MgO samples coated with $NaNO_3$/$NaNO_2$ as promoters for CO_2 capture at intermediate temperatures. The CO_2 capture capacity and kinetics were examined under designed conditions. The use of lab-conditions for new materials is quite common and some studies only reported the performance of MgO sorbents under pure CO_2 stream. Although highly stable capture performance of CO_2 sorbents over cycles were reported, their testing conditions have been criticized to be "unrealistic" or "too mild" [14,33,34]. Thus, use of harsh conditions, especially in the calcination stage is highly suggested. Therefore, in this work, firstly, we conducted the screening tests to find out the optimal synthesis and operation conditions under 0.85 bar of CO_2 (balanced with 0.15 bar of N_2). Then, the performance of the best sorbents under pure CO_2 and lower partial pressure of CO_2 were tested as reference or comparison. Finally, we tested the best sorbents under more harsh conditions or wet conditions over carbonation-decarbonation cycles. The specific objectives and strategies included: 1) to thoroughly analyze the characterizations and structure of synthesized MgO sorbents; 2) to find out the optimal conditions for the preparation of the best synthetic materials, by studying the effect of hydrothermal solution pH and loadings of promoters; 3) to investigate the influence of operational temperature and CO_2 partial pressure, and examine the multi-cycle

performance under both ideal and realistic conditions; 4) to compare the sorbents in this work with other MgO-based CO_2 sorbents from the open literature; and 5) to propose the mechanisms of sorption through analyzing the sorption kinetics data in depth.

2. Materials and methods

2.1. Chemicals and materials

All chemical reagents used in this study are of analytical grade or higher. Magnesium acetate tetrahydrate ($Mg(CH_3COO)_2 \cdot 4H_2O$, 98%) was purchased from Alfa Aesar (Ward Hill, MA, USA). Sodium nitrate ($NaNO_3$, 99%), sodium nitrite ($NaNO_2$, 99%), urea ($CO(NH_2)_2$, 99%), 25-28% ammonia solution, and acetic acid (99.5%) were obtained from Xilong Co. (Guangdong, China). The water utilized in the experiments was deionized water (18 MΩ·cm). Pure CO_2 and N_2 (Qianxi Co., China; 99.999%) were mixed to prepare simulated flue gas.

2.2. Fabrication of mesoporous MgO

The mesoporous MgO was synthesized through a hydrothermal process followed by calcination. In a typical experiment, $Mg(CH_3COO)_2 \cdot 4H_2O$ (0.08 mol) and urea (0.24 mol) were dissolved into 50 mL deionized water. The morphology of MgO was controlled via varying the initial pH of the Mg^{2+} and urea mixture. The pH of the hydrothermal solution was 8.2 but can be adjusted to 5.0 and 6.0 using acetic acid (99.5%), or to 9.0 and 10.0 using concentrated ammonia solution (25-28%). The mixture was then transferred into a 100 mL Teflon autoclave and heated at 180 °C in a muffle furnace for 5 h. After cooling to room temperature, the white precipitates were collected through filtration and washed with deionized water and absolute ethanol, then dried at 60 °C for 4 h. The white powder was then calcined in air for 5 hours at 500 °C to obtain mesoporous MgO with different morphologies.

To produce a coating of promoters, the calcined MgO was dispersed in ethanol solution of the designed alkali metal nitrates/nitrites. Typically, 2 g of MgO was mixed into 50 mL of ethanol with the required dose of $NaNO_3$ or $NaNO_2$ (both from stock solutions). The mixture was then ultrasonicated for 1 h followed by evaporation of ethanol at 60 °C overnight. The $MgO/NaNO_3/NaNO_2$ molar ratio was denoted as 1:*x*:*y*; *x* was varied from 0 to 0.15 to test the effect of $NaNO_3$ content with *y* fixed at 0, while *y* was controlled from 0 to 0.08 to examine the effect of $NaNO_2$ with *x* fixed at 0.07.

2.3. Materials characterization

Morphological studies on the samples were carried out using scanning electron microscopy (SEM, Zeiss MERLIN VP Compact). Powder X-ray diffractometer (XRD) analysis was conducted using a Dmax/2500 XRD (Rigaku, Japan) using Cu $K\alpha$ radiation at a scan rate (2θ) of $8°\cdot min^{-1}$. The Brunauer-Emmett-Teller (BET) surface area was measured by N_2 physisorption on a Quantachrome autosorb iQ-C instrument. Pore volume and pore size distribution were obtained following the Barrett-Joyner-Halenda (BJH) method.

2.4. Absorption and cycle tests

CO_2 capture behavior was examined using a Thermogravimetric Analyzer (TGA, TA Instruments, TGA-Q50) under a flow of 0.85 bar dry CO_2 at atmospheric pressure (total flow rate = 110 $mL\cdot min^{-1}$ with 0.15 bar N_2). For each run, around 20 mg of dry sample was loaded into the TGA, and subjected to a precalcination at 450 °C for 30 min under pure N_2 (110 $mL\cdot min^{-1}$) to remove the preabsorbed species. When the chamber temperature reached the designated value, the measurement was initiated by switching the sample gas from N_2 to CO_2. To test the effect of CO_2 partial pressure, the sample gas was changed from 0.85 bar to 0.70, 0.50 and 0.30 bar, respectively. To test the regenerability of the samples, the system was changed

from 0.85 bar of CO_2 at 325 °C (or 350 °C) for 30 min for carbonation, to 1 bar of N_2 at 400 °C for 20 min for calcination over 15 cycles, and this scenario was named as "S1". To test more harsh conditions, we also conducted the cycle tests under three more scenarios and their carbonation and decarbonation conditions (temperature/partial pressure of CO_2) are: S2: Carbonated at 350 °C/0.85 bar and decarbonated at 450 °C/1 bar; S3: Carbonated at 325 °C/0.3 bar and decarbonated at 450 °C/1 bar; S4: Carbonated at 325 °C/0.3 bar (with ~0.01 bar of steam) and decarbonated at 450 °C/1 bar. For all scenarios, the carbonation and decarbonation time are 30 and 20 min, respectively.

3. Results and discussion

3.1. Characterizations

3.1.1. Characterizations and morphology control of MgO

The powders obtained after the hydrothermal process with a solution pH range of 5.0-10.0 were examined by XRD and the patterns are given in Fig. 1a. All these peaks can be indexed as pure hexagonal-symmetry $MgCO_3$ (JCPDS No. 08-0479). The crystallite sizes estimated by Scherrer Equation with respect to the *hkl* Miller indices (104), (113) and (116) are tabulated in Table S1 (Supporting Information). It is observed that the increase of solution pH from 5.0 to 9.0 resulted in decreasing crystallite sizes of $MgCO_3$, while the size increased when pH changed from 9.0 to 10.0, suggesting that the smallest crystallite size can be obtained at pH 9.0. Moreover, as shown in Fig. 1a, the peak with highest intensity changed from (104) to (113) facet, when pH increased from 8.2 to 9.0 and higher. Therefore, the increase of pH appeared to increase the intensity of the (113) reflection, indicating a promotion in the crystal growth in the (113) direction.

[Fig. 1]

[Table 1]

These $MgCO_3$ powders were used as precursors to prepare mesoporous MgO by calcination at 500 °C for 5 h. For the calcined samples, the peaks present in XRD patterns in Fig. 1b correspond to the cubic MgO (JCPDS No. 45-0946). The crystallite sizes estimated by Scherrer equation with respect to the *hkl* Miller indices (111), (200) and (220) are tabulated in Table 1. The crystallite sizes of MgO followed the same trend of $MgCO_3$ and minimized at hydrothermal pH 9.0. A previous study also reported that the calcination does not destroy the morphology of $MgCO_3$ and for a series of precursors the smallest MgO crystals can be obtained from the smallest $MgCO_3$ crystals [13].

The micro- to nano-structural characteristics of the mesoporous MgO were further analyzed by SEM (Fig. 2). Interestingly, at hydrothermal solution pH of 5, mainly ball-like rhombohedral MgO with a diameter of 40-60 μm was obtained (Fig. 2a). The mesoporous MgO synthesized at a higher pH range (Fig. 2b-2e) exhibited a micro-rod like morphology with fan-shaped trihedral ends. It is evident that smaller sized micro-rods can be produced at pH 9.0.

[Fig. 2]

The information on BET-based specific surface area, pore volume and average pore size is summarized in Table 1. All the MgO are mesoporous materials with high BET specific surface area (> 180 $m^2 \cdot g^{-1}$), pore volume (≥ 0.39 $cm^3 \cdot g^{-1}$) and meso-pore size (5–7 nm). The MgO synthesized at hydrothermal pH 9.0 exhibited the highest BET specific surface area (230 $m^2 \cdot g^{-1}$), highest pore volume (0.49 $cm^3 \cdot g^{-1}$) and smallest pore size (5.65 nm).

Generally, the intrinsic symmetry of crystalline lattices and growth kinetics govern the shape of a crystalline nanostructure [13]. During hydrothermal processes, major reactions are proposed such as [13,35]:

$$CO(NH_2)_2 + H_2O \rightarrow CO_2 + 2NH_3 \quad (1)$$

$$NH_3 + H_2O \rightarrow NH_4^+ + OH^- \quad (2)$$

$$Mg^{2+} + 2OH^- \rightarrow Mg(OH)_2 \quad (3)$$

$$Mg(OH)_2 + CO_2 \rightarrow MgCO_3 + H_2O \quad (4)$$

The nanoscale self-assembling of $MgCO_3$ can be realized by homogeneous precipitation. Firstly, urea decomposition under hydrothermal conditions can release OH^- ions and CO_2 molecules (Eqns. 1-2) [13]. Subsequently, the Mg^{2+} can precipitate out rapidly with $Mg(OH)_2$ nuclei formed according to Eqn. 3, then transformed to $MgCO_3$ (Eqn. 4). Apparently, the formation of $Mg(OH)_2$ and the decomposition of urea are pH dependent. It has been reported that during the initial stage of hydrothermal treatment of a mixture of Mg^{2+} and urea, amorphous seeds (termed xMgCO$_3$·Mg(OH)$_2$) can form as intermediates [36,37]. These seeds can then be rearranged into more stable structures through a dissolution-formation process, and the final morphology/structure depends on various parameters including temperature, growth time, solution pH, concentration of free carbonate ion and pressure [35-37]. The anisotropy of growth rates in different crystallographic directions controls the final morphologies of materials. The newly formed crystallites can be self-assembled on the existing nuclei [13]. In this study, a clear solution mixture of Mg^{2+} and urea was observed when pH was adjusted to 5.0, 6.0, 8.2 and 9.0, while the solution turned turbid at pH 10.0 indicating the presence of amorphous seeds, which

may explain the larger size in the case of pH 10.0 since the seeds exist before the hydrothermal treatment. While in the pH range of 5.0-9.0, since less CO_3^{2-} or OH^- available at lower pH, the nucleation rate of Mg is limited and the nuclei are prone to assemble into larger particles [38]. Therefore, in this study, pH 9.0 is the optimal pH to synthesize MgO with smallest crystallite size.

3.1.2. Characterizations of MgO promoted with $NaNO_3$/$NaNO_2$

The mesoporous MgO-pH9.0 coated with $NaNO_3$ and $NaNO_3$+$NaNO_2$ were analyzed by XRD as shown in Fig. 3a and 3b, respectively. The spectra of Fig. 3a reveal both components: MgO skeleton and $NaNO_3$ as promoter in the sample before absorption. The well-crystallized $MgCO_3$ particles were produced after the reaction with CO_2. After regeneration of the sorbents at the 15th cycle, there was no $MgCO_3$ identified, suggesting a full decomposition during regeneration. Three components of MgO-$NaNO_3$+$NaNO_2$ were also found in the sample before sorption as shown in Fig. 3b. The formation and full decomposition of $MgCO_3$ was also confirmed in the spectra of sorbent after absorption and after regeneration. For both sorbents, all the XRD results indicated that no double carbonates ($Na_2Mg(CO_3)_2$) were formed during the sorption/regeneration processes. In addition, sharper peaks were observed in the regenerated samples than the fresh samples, and details of Miller indices (111), (200) and (220) of MgO based on Scherrer Equation (as shown in Table 1) demonstrated that crystallite size was increased after regeneration.

[Fig. 3]

Fig. 4 presents the SEM images of raw MgO-pH9.0 and the promoted MgO. Clear cracks and meso-pores can be observed for the mesoporous MgO as shown in Fig. 4a. Coating using $NaNO_3$

or $NaNO_3$+$NaNO_2$ did not change the overall morphology or size of MgO according to Fig. 4b and 4c, and specific surface area and pore size were examined to reveal the change of the textural properties.

[Fig. 4]

The N_2 adsorption/desorption isotherms and pore size distributions of mesoporous MgO-pH9.0 and promoted MgO are shown in Fig. 5. Irreversible isotherms were recorded for these materials, and they were all Type IVa isotherms (according to the 2015 IUPAC classification), which are typically given by mesoporous sorbents [39]. A sharp hysteresis loop of Type H2b was given by the mesoporous MgO, suggesting the robust network effects in the pore structure. Type H2b is commonly reported for hydrothermally-treated materials [39], while the loops produced for the promoted MgO are more likely classified as Type H4 hysteresis, which is often found with aggregated crystals, indicating the loss of pores due to the covering of promoters. This was again confirmed by the significant reduction of both specific surface area and pore volume, and the increased crystallite size of MgO (as shown in Table 1). The pore size distribution of these materials is quite narrow (inset of Fig. 5), and after adding the promoters, the average pore size decreased from 5.65 nm to 3.94 nm with pore volume decreased from 0.49 to 0.08 $cm^3 \cdot g^{-1}$, implying the crystals of promoters may have occupied the mesoporous pores.

[Fig. 5]

3.2. CO_2 sorption behavior

3.2.1. Effect of hydrothermal solution pH

Fig. 6 shows the uptake of CO_2 by mesoporous MgO synthesized at various hydrothermal solution pH with a fixed $NaNO_3$ loading (x=0.07) at 325 °C. Evidently, more alkaline

hydrothermal solution (at pH range of 5.0 to 9.0) could produce MgO with higher CO_2 capture capacity, and the CO_2 uptake of a batch produced with pH 9.0 (MgO-pH9.0) reached up to 15.2 $mmol \cdot g^{-1}$ in 70 min. The batch prepared at pH 10.0 exhibited comparable performance with a batch prepared at pH 8.2, despite relatively faster kinetics at initial state. Thus, the optimal hydrothermal solution pH for MgO synthesis is determined to be 9.0 and MgO-pH9.0 was used for further study on the promoting effects.

[Fig. 6]

As discussed above, the mesoporous MgO-pH9.0 has the smallest crystallite size, and the largest specific surface area and pore volume. Though the introduction of promoters can significantly reduce the surface area and block the mesoporous pores, the overall performance of promoted MgO is still highly dependent on the morphology and textural structure of the MgO. These results imply that the structure of MgO skeleton plays a key role and its large mesoporous pores are activated when promoters melt.

3.2.2. Effect of content of $NaNO_3$/$NaNO_2$

As shown in Fig. 7, the introduction of $NaNO_3$ and $NaNO_2$ as promoters led to a significant enhancement for CO_2 uptake compared to pure MgO-pH9.0. Thus, in Fig. 7a, the CO_2 capture capacity of mesoporous MgO was only 0.29 $mmol \cdot g^{-1}$ at 325 °C in 70 min. While the addition of 0.05 mol of $NaNO_3$ into 1 mol of MgO (x=0.05) improved the capacity over 40 times (up to 11.7 $mmol \cdot g^{-1}$). The uptake was further increased to 15.2 $mmol \cdot g^{-1}$ when $NaNO_3$ loading ratio x=0.07 and then suppressed to 10.7 $mmol \cdot g^{-1}$ when x=0.15.

[Fig. 7]

Furthermore, the addition of $NaNO_2$ into MgO-$NaNO_3$ led to a synergetic effect and boosted its CO_2 capture capacity at 350 °C. The $NaNO_3$ content was fixed as x=0.07 to study the effect of $NaNO_2$ addition. As shown in Fig. 7b, the MgO solely promoted by $NaNO_3$ (x=0.07, y=0) only exhibited a CO_2 uptake of 5.7 mmol·g^{-1}. While the MgO solely promoted by $NaNO_2$ (x=0, y=0.04) showed extremely low uptake (1.1 mmol·g^{-1}), indicating the improvement of either single promoter was limited at this temperature. However, when the $NaNO_2$ loading ratio y increased from 0.02 to 0.04, the CO_2 uptake increased from 12.8 mmol·g^{-1} to 19.8 mmol·g^{-1}. Again, with higher loading (y=0.08), the overall capacity decreased, suggesting the optimal $NaNO_2$ loading ratio y is around 0.04.

In this study, the highest CO_2 uptake of MgO-$NaNO_3$ is 15.2 mmol·g^{-1} at 325 °C, corresponding to MgO conversion of 70.4%, while the highest CO_2 uptake of MgO-$NaNO_3$+$NaNO_2$ is 19.8 mmol·g^{-1} at 350 °C with a MgO conversion of nearly 96%. Thus, it is clear that an optimal dosage of promoters exists. The addition of promoters induces a sharp drop of specific surface area of mesoporous MgO (as shown in Table 1), suggesting the strong wetting and covering effect of $NaNO_3$/$NaNO_2$. Higher loadings of promoter can suppress the specific surface even more [18]. Triple phase boundaries exist in between the solid MgO, molten (or pre-molten) promoters and gaseous CO_2. A low dose of promoter is not enough to penetrate the phase boundaries or the rigid structure of formed carbonates on the surface. However, excessive loadings of promoters do not enhance the interactions further due to the limited CO_2 solubility in promoters (the reported solubility is ~10^{-3} mol·L^{-1} at 300 ºC[40]). In addition, the too-high coverage of promoters on MgO will inhibit the initial contact between MgO and CO_2, which is also an important factor in enhancing the promoting effect as discussed below (Section 3.2 Stage

I). Thus, both too-low and too-high doses of promoters can cause a decrease in the sorption capacity and the CO_2 capture rate.

3.2.3. Effect of temperature

The influence of temperature on the CO_2 sorption rate and CO_2 uptake on MgO-pH9.0 promoted by $NaNO_3$ and $NaNO_3$+$NaNO_2$ was examined over a temperature range of 275 °C to 375 °C. For MgO promoted by $NaNO_3$ as shown in Fig. 8a, when temperature increased from 275 °C to 325 °C, the CO_2 sorption capacity increased from 9.4 to 15.2 mmol·g^{-1}. Further increase of temperature inhibited the CO_2 uptake and led to a severe decrease of capacity down to 0.2 mmol·g^{-1} at 375 °C in 70 min, which is almost the same as the capacity of unmodified MgO, indicating nearly no CO_2 sorption. Based on a 4-h kinetics study as shown in Fig. S1 in SI, equilibrium has not been reached until ~ 150 min at temperature 275 °C to 325 °C.

[Fig. 8]

Fig. 8b summarizes the CO_2 capture performance of MgO promoted by $NaNO_3$+$NaNO_2$ at different temperatures. The highest uptake was recorded at 350 °C even though the evidently faster initial kinetics were observed at lower temperatures (275-325 °C). The sorption equilibrium was reached within nearly 20 min at temperature 275-325 °C, and within 40 min for 350 °C, which is much faster than the MgO with single $NaNO_3$ promoter. Again, suppressed CO_2 uptake occurred at a higher temperature (375 °C).

The theoretical melting point for $NaNO_3$ and $NaNO_2$ are 308 and 271 °C, respectively [30], and the reported eutectic melting point of their mixture is ~ 185 °C [41]. It has been observed that nitrate/nitrite salts exhibited pre-molten phenomena, during which a continuous solid-state transition occurred even prior to reaching the melting point [42]. Based on the results in Fig. 8a,

the temperature of 275 °C is high enough for $NaNO_3$ to promote the MgO sorbent, suggesting that the promoters can be activated at a pre-molten state.

The uptake performance is strongly affected by temperature. Increased temperature can cause a double effect on the interactions between CO_2 and promoted MgO. Positively, higher temperatures enable faster kinetics for more rapid reaction between CO_2 and MgO; negatively, especially when the temperature exceeds the optimal value, several problems can occur: 1) the solubility of CO_2 in the molten salt decreases with increasing temperature [40,43], resulting in less CO_2 being dissolved into the molten promoter at elevated temperatures. The relatively higher concentration of available CO_2 dissolved in promoters may explain the faster initial kinetics at 275-325 °C than that at 350-375 °C in Fig. 8b; and 2) the enthalpy change of $MgCO_3$ formation ($CO_2+MgO \rightarrow MgCO_3$, $\Delta H_{300K}= -106$ kJ·mol^{-1}) is negative [44], thus thermodynamically, the conversion to $MgCO_3$ is inhibited and its decomposition is enhanced at higher temperatures. Taken together, the overall performance of a sorbent depends on the balance of these effects, and an optimal operating temperature exists for a promoted MgO. In this study, the optimal value for MgO-$NaNO_3$ and MgO-$NaNO_3$+$NaNO_2$ are 325 °C and 350 °C, respectively. This can be explored further by breaking down the interactions of CO_2 and MgO. Firstly, both reactants are dissolved into the molten or pre-molten promoters, resulting in a decrease of enthalpy (ΔH) for the $MgCO_3$ formation [43,45]; moreover, the MgO dissolution into the promoters is more predominant than CO_2 dissolution, and induces an overall decrease of entropy (ΔS), which is also negative in terms of the $MgCO_3$ formation [29]. The dissolution of MgO in $NaNO_3$ was proven and the measured solubility was 10^{-7} mol·kg^{-1} at 300 ºC [46] and 3.1 $\times 10^{-2}$ mol·kg^{-1} at 450 ºC [47]. Previous study demonstrated that for the promoted MgO, the alterations of the enthalpy and entropy lead to a transition point shift to higher temperatures for

$MgCO_3$ formation [29]. Apparently in this study, the introduction of $NaNO_3$ produces an optimal $MgCO_3$ formation temperature up to ~325 °C and the addition of $NaNO_2$ raises this temperature point even higher (350 °C). Interestingly, a similar trend was reported for MgO nanoclusters promoted by nitrates solely and nitrates/nitrites mixtures [29].

3.2.4. Effect of CO_2 partial pressure

The CO_2 partial pressure effects on the variations in uptake were examined at four different CO_2 levels at fixed temperature for promoted MgO-pH9.0. Evidently for both materials, MgO-$NaNO_3$ (as shown in Fig. 9a) and MgO-$NaNO_3$+$NaNO_2$ (Fig. 9b), the CO_2 uptake was strongly dependent on the partial pressure of CO_2. For both materials, the overall trend was that lower uptake was found at decreased partial pressure of CO_2. For both sorbents, the use of pure CO_2 during carbonation could only fasten the kinetics with slightly enhancement on the final CO_2 uptake within 70 min under otherwise identical conditions. The uptake of MgO-$NaNO_3$+$NaNO_2$ was even more sensitive to these influences than MgO-$NaNO_3$, and nearly no transition was observed for MgO-$NaNO_3$+$NaNO_2$ at a CO_2 partial pressure of 0.30 bar at 350 °C. However, its uptake increased to 9.9 $mmol \cdot g^{-1}$ at 0.30 bar of CO_2 when temperature decreased to 325 °C (Fig. 9b), suggesting that the uptake was also strongly temperature-dependent. Harada reported a similar observation that with 0.30 bar of CO_2, the uptake by MgO nanoclusters coated with $LiNO_3$+(Na-K)NO_2 did not exceed 0.3 $mmol \cdot g^{-1}$ at 340 °C, while they achieved more than 13 $mmol \cdot g^{-1}$ at 300 °C [29]. Since higher temperature inhibits the dissolution of CO_2 into promoters, the low partial pressure of CO_2 leads to insufficient CO_2 available for sorbents and the resulting effect is suppressed capture. The observations in the present study and the available literature all suggest that with lower CO_2 partial pressure (less than 0.50 bar), a relatively lower temperature

is more favorable for CO_2 trapping. Thus, the overall performance of MgO sorbents is not only strongly temperature-dependent, but also CO_2-partial pressure-dependent.

[Fig. 9]

3.2.5. Stability of the sorbents over cycles under idea and harsh conditions

The regenerability of MgO-$NaNO_3$ and $NaNO_3$+$NaNO_2$ were examined by repeating the cycle of CO_2 sorption and desorption as shown in Fig. 10. Here, the program for the CO_2 sorption was 30 min with CO_2 partial pressure of 0.85 bar, at temperature of 325 °C for MgO-$NaNO_3$ and 350 °C for MgO-$NaNO_3$+$NaNO_2$, respectively. The decarbonation step was conducted at 400 °C with pure N_2 for 20 min for both sorbents. In both cases, the uptake of CO_2 decreased gradually in the first 4 or 5 cycles, then was quite stable with minimal further degradation. The sorption capacity dropped from 12.4 $mmol \cdot g^{-1}$ at the 1st cycle to 5.6 $mmol \cdot g^{-1}$ at the 15th cycle for MgO-$NaNO_3$ and from 18.9 $mmol \cdot g^{-1}$ to 8.6 $mmol \cdot g^{-1}$ for MgO-$NaNO_3$+$NaNO_2$. Gradual deterioration over repeated cycles was reported for some other MgO-based sorbents [14,18,29,31]. A sintering effect due to phase transition is suggested to be the main reason for the deactivation [14,27]. In addition, $MgCO_3$ has a low Tammann temperature (the empirical temperature at which bulk sintering effect becomes significant, $T_{Tammann}$ is usually half of the absolute melting point), which in this case is ~180 °C, which is lower than either the temperature of carbonation (350 °C) or calcination (400 °C). In this study, the specific surface area, pore volume, and average pore size of sorbents decreased with increasing cycles as shown in Table 1. In addition, the XRD profiles in Fig. 3 confirm that the crystallite sizes of sorbents increased after 15 cycles. Fig. 11 presents the SEM images of the sorbents after sorption (Fig. 11a and 11c) and after regeneration (Fig. 11b and 11d). It is evident that after reaction with CO_2, the surface of MgO-$NaNO_3$ became more thorn-like (Fig. 11a) and the surface of MgO-

$NaNO_3$+$NaNO_2$ became more knobby (Fig. 11c). These changes to produce a rougher surface may be a result of the much lower mass density of $MgCO_3$ (2.96 $g \cdot cm^3$) than that of MgO (3.58 $g \cdot cm^3$). After regeneration at the 15^{th} cycle, the pores became much larger (with diameter >100 nm, as shown in Fig. 11b and 11d) for both sorbents, suggesting that the mesoporous structures were all damaged. Therefore, for the mesoporous MgO sorbents in this study, the destruction of the MgO skeleton is also an important contributor to the material deactivation during repeated cycles. In addition, since molten promoters can be decomposed to generate O^{2-} [48], the gradual loss of active promoters can also be a reason for the decay of capacity over cycles.

[Fig. 10]

[Fig. 11]

We also tested the best sorbent under more harsh and realistic conditions as shown in Fig. 12. It is evident that when the test conditions changed from ideal scenario (S1) to more harsh conditions (S2-4), the capacity of the sorbents were suppressed significantly (detailed data can also be found in Table 2) due to more severe sintering effects [34,49]. For S2-4, since pure CO_2 stream was used as regeneration gas, an "over-carbonation" was observed during the temperature ramping process of decarbonation as shown in Fig. S2 in SI. The decarbonation did not initialize until the temperature reached 428 ºC, thereby we used 450 ºC as the calcination temperature to make sure completed regeneration. In addition, the weight gain due to the "over-carbonation" was not included as the CO_2 uptake over cycles. After 15 cycles in S1, the BET surface area and pore volume for the samples were 18 $m^2 \cdot g^{-1}$ and 0.032 $cm^3 \cdot g^{-1}$, respectively, yet the values were further decreased to 15 $m^2 \cdot g^{-1}$ and 0.023 $cm^3 \cdot g^{-1}$ for S2, suggesting more severe deactivation of the sorbents. It is noteworthy that water vapor can improve the cyclic performance of the

sorbents according to the results of S3 (dry) and S4 (wet). This trend is in agreement with previous study [49] and the enhancement under wet conditions was mainly due to the formation of transient $Mg(OH)_2$, which is more powerful than MgO for CO_2 capture [14].

[Fig. 12]

3.2.6. Comparison with other MgO sorbents

The CO_2 sorption performance of several synthesized MgO samples with different promoters was compared and summarized in Table S2 in SI. The capture capacity of synthesized mesoporous MgO [27] is only 0.5 $mmol \cdot g^{-1}$, which is comparable to the value found in this study (0.29 $mmol \cdot g^{-1}$), indicating the poor reactivity of MgO. Utilization of Al_2O_3 as inert support can increase the capacity up to 1.8 $mmol \cdot g^{-1}$ due to enlarged specific surface area [50]. The addition of Na_2CO_3 or K_2CO_3 into the composite can facilitate the formation of $Na_2Mg(CO_3)_2$ or $K_2Mg(CO_3)_2$, but still the promotion effect is not significant and the conversion of MgO is far below its theoretical limit [14,25,51]. Not until Zhang et al. discovered the role of $NaNO_3$ as a PTC with a conversion of MgO increasing up to 75% [18,26], did the use of alkali metal nitrates/nitrites become attractive to promote the MgO-based CO_2 sorbent [14,27-29,31,51]. It was demonstrated that the combination of two or three promoters can work even better, and the commonly used pairs/groups include double sodium salts ($NaNO_3$ and Na_2CO_3) [14,51], mixtures of alkaline metal nitrates (Li-Na-K)NO_3 [28,31], or mixtures of alkaline metal nitrates and nitrites $LiNO_3$+(Na-K)NO_2 [29]. In these papers, the promoting effect was observed on different types of MgO, i.e., synthesized mesoporous MgO, commercial MgO powder, ball-milled MgO powder, and MgO nanoclusters. In the present work, the mesoporous MgO promoted by $NaNO_3$+$NaNO_2$ exhibited a CO_2 capture capacity as high as 19.8 $mmol \cdot g^{-1}$ within only 50 min, making it the most efficient MgO-based CO_2 sorbent with highest capacity and

fastest sorption rate demonstrated so far. The pore size (5-6 nm) of the MgO skeleton is smaller than the reported values in literatures (usually 15-25 nm) [14,52]. Previous study suggested that for mesoporous materials, the capillary condensation caused by the nanoscale channels could also contribute to CO_2 capture [53,54]. Therefore, we hypothesize that the unique mesoporous structure of MgO in this study may provide a strong capillary condensation effect resulting in an improved CO_2 capture capacity. The capture performance over cycles for sorbents were also summarized in Table S2. Under ideal conditions, the sorbent in this work exhibited highest capacity but worse stability over cycles compared to MgO-(Li, K)NO_3+(Na-K)$_2CO_2$ sorbent synthesized by precipitation method [34]. Under more harsh conditions as S3 and S4, the best sorbent in this study showed high capacity as 4.8 and 5 $mmol \cdot g^{-1}$, respectively, even after 15 cycles.

3.3. Reaction mechanisms and the role of promoters

Fig. 13a and 13b focus on the details of CO_2 sorption kinetics for the 1st cycle and 15th cycle of the two sorbents. The sorption rate, which is calculated as the first order derivative of CO_2 uptake variation with respect to time, was also plotted as dashed lines to allow the analysis of reaction mechanisms [55]. As shown in Fig. 13a, for the untreated MgO, the sorption rate peaked within 1 min and then stabilized to ~0 quickly. For both promoted MgO samples, the sorption rate clearly exhibited a "three-stage" evolution, indicating the potential dynamic variations along with reaction time. Their sorption rate experienced a similar peak within 1 min (Stage I), then held stable for nearly 1.5 min (Stage II) followed by a remarkable rebound lasting for more than 20 min (Stage III). To better discuss the phenomena and elucidate the mechanisms, we here focus on the interactions between MgO, promoters and CO_2 in these three stages.

[Fig. 13]

Stage I: initiating interactions between CO_2 and exposed MgO. The rather large similar peaks for pristine MgO and promoted MgO suggest intensive interactions between CO_2 and exposed MgO in this initial stage (< 1 min). This carbonation reaction can produce a unidentate carbonate layer [28]. The rigid structure of this carbonate layer can constrain the generation of carbonate ions (CO_3^{2-}), resulting in an inhibition of further carbonation [15].

Stage II: generation and accumulation of Mg^{2+} and CO_3^{2-}. The dissolution of MgO into nitrates/nitrites breaks the strong ionic bonds in the bulk MgO and generates solvated ionic pairs of magnesium ions (Mg^{2+}) and oxide ions (O^{2-}) [29]. The molten promoters can produce high concentration of O^{2-} (~ 2×10^{-7} mole·L^{-1} or higher) [56], and usually $NaNO_2$ can generate more O^{2-} than can $NaNO_3$ [48]. The O^{2-} is predominantly produced from promoters melting rather than MgO dissolution. On the other hand, CO_2 molecules can be dissolved into molten promoters with a solubility at scale of ~10^{-3} mol·L^{-1} at 300 ℃ [40]. Thus, the molten promoters may serve as a sink for the generated O^{2-} and accumulated CO_2 molecules to produce CO_3^{2-}. In this work (Fig. 13a), a higher amount of O^{2-} is expected in the MgO-$NaNO_3$+$NaNO_2$, while it shares a comparable value at Stage II with MgO-$NaNO_3$, suggesting the O^{2-} generating is not the rate-limiting step. A recent study proposed that the generation of Mg^{2+} is the rate-limiting step, since it is the most energetically unfavorable process according to density functional theory (DFT) [18]. Thus, it is likely that the slow generation of Mg^{2+} holds the material staying in Stage II for nearly 1.5 min.

Stage III: fast carbonation. Sufficient Mg^{2+} and CO_3^{2-} in molten promoters trigger the fast nucleation of $MgCO_3$ crystals. Moreover, the O^{2-} can also activate the unidentate carbonates through oxygen exchanges, thereby smoothing the conversion of unidentate carbonates to CO_3^{2-} [28,57]. The mesoporous MgO skeleton also contains some lattice defects of variances and

mesoporous pores, which may also contribute to the rapid growth of $MgCO_3$ [28,58]. In this work, the sorption rate of MgO-$NaNO_3$+$NaNO_2$ exhibits a larger hump than that of MgO-$NaNO_3$, indicating the addition of nitrite can further enhance the promoting effect. It has been reported that MgO in molten nitrite can generate magnesium nitro ($Mg–NO_2$) or nitrato ($Mg–O–NO_2$, $Mg–O_2–NO$, $(Mg–O)_2=NO$), which are all capable of creating lattice defects to enhance the nucleation of $MgCO_3$ [29].

"Three stages" in 15th cycle. Fig. 13b depicts the sorption kinetics and sorption rate for both sorbents in the 15th cycle. Compared to the 1st cycle, two smaller peaks were observed in Stage I, suggesting that there was less exposed active MgO after many repeated cycles. Thus, the reduced surface area, pore size and damaged MgO structure all support this hypothesis. Stage II also lasted for longer time than the one seen with the 1st cycle, implying that the deactivation of sorbents inhibited the accumulation of Mg^{2+} and CO_3^{2-}. The sorption rate in Stage III also decreased significantly due to suppressed carbonation.

In this study, based on the content, the $NaNO_3$ and $NaNO_2$ were used as major promoter and sub-promoter (or co-promoter), respectively. As proposed in the previous publication, molten $NaNO_3$ mainly served as a medium in which both CO_2 and MgO can dissolve [14,18,26,47]. Based on the results in this work, the roles of $NaNO_2$ as sub-promoters mainly include: 1) alter the eutectic melting point for promoters mixture; 2) change the optimal temperature for carbonation reaction due to the alterations of the enthalpy and entropy for $MgCO_3$ formation (as discussed in Section 3.2.3); 3) generate more O^{2-} during Stage II; 4) molten nitrite can generate magnesium nitro ($Mg–NO_2$) or nitrato ($Mg–O–NO_2$, $Mg–O_2–NO$, $(Mg–O)_2=NO$) to enhance the nucleation of $MgCO_3$.

4. Conclusions

This work provides a detailed investigation of the synthesis and performance of a series of MgO-based CO_2 sorbents. The major findings are summarized as follows:

1) Mesoporous MgO with high specific surface area and high pore volume can be synthesized through a simple hydrothermal method. The morphology of the materials can be tuned by varying the solution pH. A pH of 9.0 maximized the surface area and pore size and, therefore, produced the highest CO_2 uptake for the promoted sorbents;

2) With a molar ratio of 1:0.07 and at 325 °C, the MgO-$NaNO_3$ sorbent can uptake the highest amount of CO_2 from an 85% CO_2 stream, i.e., 15.2 $mmol \cdot g^{-1}$, corresponding to a MgO conversion of 70.4%. The highest uptake of MgO-$NaNO_3$+$NaNO_2$, 19.8 $mmol \cdot g^{-1}$, was detected with a molar ratio of 1:0.07:0.04 and at 350 °C, equal to an MgO conversion of ~96%. This is, to the best of our knowledge, the highest CO_2 capture capacity reported in the open literature for MgO;

3) For both promoted sorbents, when temperature is fixed, lower CO_2 uptake was found with decreasing CO_2 partial pressure. While with lower CO_2 partial pressure (less than 0.50 bar), a relatively lower temperature is more favorable for CO_2 capture;

4) Gradual deterioration of sorbents was found over the first 5 cycles followed by stable regenerability through the 5^{th}-15^{th} cycles. A sintering effect due to phase transition and transformation of mesoporous structure of MgO might be the main reason for the deactivation. More severe sintering effect under harsh decarbonation conditions suppressed the stability of the sorbents over cycles;

5) The interaction between promoted MgO and CO_2 exhibited a "three-stage" evolution: Stage I: initiating interactions between CO_2 and exposed MgO; Stage II: generation and accumulation of Mg^{2+} and CO_3^{2-}; and Stage III: fast carbonation.

5. Acknowledgements

This work was supported by the National Natural Science Foundation of China (grant number: 51506112) and the Tsinghua University Initiative Scientific Research Program (grant number: 20161080094). X. Zhao is grateful for the support by General Financial Grant from the China Postdoctoral Science Foundation (grant number: 2016M601056).

References:

[1] G. Lomax, M. Workman, T. Lenton, N. Shah, Reframing the policy approach to greenhouse gas removal technologies, Energy Policy 78 (2015) 125-136.
[2] M. Zhao, A.I. Minett, A.T. Harris, A review of techno-economic models for the retrofitting of conventional pulverised-coal power plants for post-combustion capture (PCC) of CO_2, Energ. Environ. Sci. 6 (2013) 25-40.
[3] G.T. Rochelle, Amine scrubbing for CO_2 capture, Science 325 (2009) 1652-1654.
[4] M. Ramezan, T.J. Skone, N.y. Nsakala, G. Liljedahl, L. Gearhart, R. Hestermann, B. Rederstorff, Carbon dioxide capture from existing coal-fired power plants, National Energy Technology Laboratory, DOE/NETL Report (2007).
[5] J. Wang, L. Huang, R. Yang, Z. Zhang, J. Wu, Y. Gao, Q. Wang, D. O'Hare, Z. Zhong, Recent advances in solid sorbents for CO_2 capture and new development trends, Energ. Environ. Sci. 7 (2014) 3478-3518.
[6] A.M. Kierzkowska, R. Pacciani, C.R. Müller, CaO-based CO_2 sorbents: From fundamentals to the development of new, highly effective materials, ChemSusChem 6 (2013) 1130-1148.
[7] G. Grasa, B. González, M. Alonso, J.C. Abanades, Comparison of CaO-based synthetic CO_2 sorbents under realistic calcination conditions, Energ. Fuel. 21 (2007) 3560-3562.
[8] V. Manovic, E.J. Anthony, Steam reactivation of spent CaO-based sorbent for multiple CO_2 capture cycles, Environ. Sci. Technol. 41 (2007) 1420-1425.
[9] G.S. Grasa, J.C. Abanades, CO_2 capture capacity of CaO in long series of carbonation/calcination cycles, Ind. Eng. Chem. Res. 45 (2006) 8846-8851.
[10] S. Choi, J.H. Drese, C.W. Jones, Adsorbent materials for carbon dioxide capture from large anthropogenic point sources, ChemSusChem 2 (2009) 796-854.
[11] B. Feng, H. An, E. Tan, Screening of CO_2 adsorbing materials for zero emission power generation systems, Energ. Fuel. 21 (2007) 426-434.

[12] C.-Y. Cao, J. Qu, F. Wei, H. Liu, W.-G. Song, Superb adsorption capacity and mechanism of flowerlike magnesium oxide nanostructures for lead and cadmium ions, ACS Appl. Mater. Inter. 4 (2012) 4283-4287.
[13] C. Yan, D. Xue, Novel self-assembled MgO nanosheet and its precursors, J. Phys. Chem. B 109 (2005) 12358-12361.
[14] A.-T. Vu, K. Ho, S. Jin, C.-H. Lee, Double sodium salt-promoted mesoporous MgO sorbent with high CO_2 sorption capacity at intermediate temperatures under dry and wet conditions, Chem. Eng. J. 291 (2016) 161-173.
[15] S. Gregg, J. Ramsay, Adsorption of carbon dioxide by magnesia studied by use of infrared and isotherm measurements, J. Chem. Soc. A (1970) 2784-2787.
[16] K. Zhang, X.S. Li, H. Chen, P. Singh, D.L. King, Molten salt promoting effect in double salt CO_2 absorbents, J. Phys. Chem. C 120 (2015) 1089-1096.
[17] L. Glasser, H.D.B. Jenkins, Lattice energies and unit cell volumes of complex ionic solids, J. Am. Chem. Soc. 122 (2000) 632-638.
[18] K. Zhang, X.S. Li, W.-Z. Li, A. Rohatgi, Y. Duan, P. Singh, L. Li, D.L. King, Phase transfer-catalyzed fast CO_2 absorption by MgO-based absorbents with high cycling capacity, Adv. Mater. Interfaces 1 (2014).
[19] M. Bhagiyalakshmi, J.Y. Lee, H.T. Jang, Synthesis of mesoporous magnesium oxide: Its application to CO_2 chemisorption, Int. J. Greenh. Gas Con. 4 (2010) 51-56.
[20] Y.Y. Li, K.K. Han, W.G. Lin, M.M. Wan, Y. Wang, J.H. Zhu, Fabrication of a new MgO/C sorbent for CO_2 capture at elevated temperature, J. Mater. Chem. A 1 (2013) 12919-12925.
[21] Y.Y. Li, M.M. Wan, W.G. Lin, Y. Wang, J.H. Zhu, A novel porous MgO sorbent fabricated through carbon insertion, J. Mater. Chem. A 2 (2014) 12014-12022.
[22] Y.Y. Li, M.M. Wan, X.D. Sun, J. Zhou, Y. Wang, J.H. Zhu, Novel fabrication of an efficient solid base: carbon-doped MgO-ZnO composite and its CO_2 capture at 473 K, J. Mater. Chem. A 3 (2015) 18535-18545.
[23] S. Walspurger, P.D. Cobden, O.V. Safonova, Y. Wu, E.J. Anthony, High CO_2 storage capacity in alkali‐promoted hydrotalcite‐based material: *In situ* detection of reversible formation of magnesium carbonate, Chem-Eur J. 16 (2010) 12694-12700.
[24] R.V. Siriwardane, R.W. Stevens Jr, Novel regenerable magnesium hydroxide sorbents for CO_2 capture at warm gas temperatures, Ind. Eng. Chem. Res. 48 (2008) 2135-2141.
[25] G. Xiao, R. Singh, A. Chaffee, P. Webley, Advanced adsorbents based on MgO and K_2CO_3 for capture of CO_2 at elevated temperatures, Int. J. Greenh. Gas Con. 5 (2011) 634-639.
[26] K. Zhang, X.S. Li, Y. Duan, D.L. King, P. Singh, L. Li, Roles of double salt formation and $NaNO_3$ in Na_2CO_3-promoted MgO absorbent for intermediate temperature CO_2 removal, Int. J. Greenh. Gas Con. 12 (2013) 351-358.
[27] A.-T. Vu, Y. Park, P.R. Jeon, C.-H. Lee, Mesoporous MgO sorbent promoted with KNO_3 for CO_2 capture at intermediate temperatures, Chem. Eng. J. 258 (2014) 254-264.
[28] T. Harada, F. Simeon, E.Z. Hamad, T.A. Hatton, Alkali metal nitrate-promoted high-capacity MgO adsorbents for regenerable CO_2 capture at moderate temperatures, Chem. Mater. 27 (2015) 1943-1949.
[29] T. Harada, T.A. Hatton, Colloidal nanoclusters of MgO coated with alkali metal nitrates/nitrites for rapid, high capacity CO_2 capture at moderate temperature, Chem. Mater. 27 (2015) 8153-8161.
[30] K.H. Stern, High temperature properties and decomposition of inorganic salts Part 3, Nitrates and Nitrites, J. Phys. Chem. Ref. Data 1 (1972) 747-772.

[31] Y. Qiao, J. Wang, Y. Zhang, W. Gao, T. Harada, L. Huang, T.A. Hatton, Q. Wang, Alkali nitrates molten salt modified commercial MgO for intermediate-temperature CO_2 capture: Optimization of the Li/Na/K ratio, Ind. Eng. Chem. Res. 56 (2017) 1509-1517.
[32] C.A. Scholes, K.H. Smith, S.E. Kentish, G.W. Stevens, CO_2 capture from pre-combustion processes—Strategies for membrane gas separation, Int. J. Greenh. Gas Con. 4 (2010) 739-755.
[33] P.T. Clough, M.E. Boot-Handford, M. Zhao, P.S. Fennell, Degradation study of a novel polymorphic sorbent under realistic post-combustion conditions, Fuel 186 (2016) 708-713.
[34] L. Wang, Z. Zhou, Y. Hu, Z. Cheng, X. Fang, Nanosheet MgO-based CO_2 sorbent promoted by mixed-alkali-metal nitrate and carbonate: Performance and mechanism, Ind. Eng. Chem. Res. 56 (2017) 5802-5812.
[35] C. Gao, W. Zhang, H. Li, L. Lang, Z. Xu, Controllable fabrication of mesoporous MgO with various morphologies and their absorption performance for toxic pollutants in water, Cryst. Growth Des. 8 (2008) 3785-3790.
[36] N. Sutradhar, A. Sinhamahapatra, S.K. Pahari, P. Pal, H.C. Bajaj, I. Mukhopadhyay, A.B. Panda, Controlled synthesis of different morphologies of MgO and their use as solid base catalysts, J. Phys. Chem. C 115 (2011) 12308-12316.
[37] K. Mitsuhashi, N. Tagami, K. Tanabe, T. Ohkubo, H. Sakai, M. Koishi, M. Abe, Synthesis of microtubes with a surface of “house of cards” structure via needlelike particles and control of their pore size, Langmuir 21 (2005) 3659-3663.
[38] Z. Zhang, Y. Zheng, Y. Ni, Z. Liu, J. Chen, X. Liang, Temperature-and pH-dependent morphology and FT− IR analysis of magnesium carbonate hydrates, J. Phys. Chem. B 110 (2006) 12969-12973.
[39] M. Thommes, K. Kaneko, V. Neimark Alexander, P. Olivier James, F. Rodriguez-Reinoso, J. Rouquerol, S.W. Sing Kenneth, Physisorption of gases, with special reference to the evaluation of surface area and pore size distribution (IUPAC Technical Report), Pure Appl. Chem., 2015, pp. 1051-1069.
[40] E. Sada, S. Katoh, H. Yoshii, I. Takemoto, N. Shiomi, Solubility of carbon dioxide in molten alkali halides and nitrates and their binary mixtures, J. Chem. Eng. Data 26 (1981) 279-281.
[41] R.W. Berg, D.H. Kerridge, P.H. Larsen, $NaNO_2$ + $NaNO_3$ phase diagram: New data from DSC and Raman spectroscopy, J. Chem. Eng. Data 51 (2006) 34-39.
[42] G.J. Janz, F.J. Kelley, J.L. Perano, Melting and pre-melting phenomena in alkali metal nitrates, J. Chem. Eng. Data 9 (1964) 133-136.
[43] A.L. Novozhilov, V.G. Bamburov, N.N. Fedotova, Solubility of carbon dioxide in molten alkali-metal nitrates, Russ. J. Inorg. Chem. 52 (2007) 1679-1681.
[44] Y. Duan, K. Zhang, X.S. Li, D.L. King, B. Li, L. Zhao, Y. Xiao, *ab initio* thermodynamic study of the CO_2 capture properties of M_2CO_3 (M = Na, K)- and $CaCO_3$-promoted MgO sorbents towards forming double salts, Aeroso Air Qual. Res. 14 (2014) 470-479.
[45] M. Fredericks, R.B. Temple, Solubility of metallic oxides and the free energy of solvation of oxide ion in molten alkali metal nitrates, Inorg. Chem. 11 (1972) 968-970.
[46] M. Fredericks, R. Temple, Solubility of metallic oxides and the free energy of solvation of oxide ion in molten alkali metal nitrates, Inorg. Chem. 11 (1972) 968-970.
[47] S.-I. Jo, Y.-I. An, K.-Y. Kim, S.-Y. Choi, J.-S. Kwak, K.-R. Oh, Y.-U. Kwon, Mechanisms of absorption and desorption of CO_2 by molten $NaNO_3$-promoted MgO, PCCP 19 (2017) 6224-6232.

[48] R.N. Kust, F.R. Duke, A Study of the Nitrate Ion Dissociation in Fused Nitrates, J. Am. Chem. Soc. 85 (1963) 3338-3340.
[49] S. Jin, K. Ho, A.-T. Vu, C.-H. Lee, Salt-composition-controlled precipitation of triple-salt-promoted MgO with enhanced CO_2 sorption rate and working capacity, Energy & Fuels (2017).
[50] K.K. Han, Y. Zhou, Y. Chun, J.H. Zhu, Efficient MgO-based mesoporous CO_2 trapper and its performance at high temperature, J. Hazard. Mater. 203–204 (2012) 341-347.
[51] C.H. Lee, S. Mun, K.B. Lee, Characteristics of Na–Mg double salt for high-temperature CO_2 sorption, Chem. Eng. J. 258 (2014) 367-373.
[52] A.O. Menezes, P.S. Silva, E. Padrón Hernández, L.E.P. Borges, M.A. Fraga, Tuning surface basic properties of nanocrystalline MgO by controlling the preparation conditions, Langmuir 26 (2010) 3382-3387.
[53] H. Zhao, J. Hu, J. Wang, L. Zhou, H. Liu, CO_2 capture by the amine-modified mesoporous materials, Acta Physico-Chimica Sinica 23 (2007) 801-806.
[54] V. Zeleňák, M. Badaničová, D. Halamová, J. Čejka, A. Zukal, N. Murafa, G. Goerigk, Amine-modified ordered mesoporous silica: Effect of pore size on carbon dioxide capture, Chem. Eng. J. 144 (2008) 336-342.
[55] G. Ji, M.Z. Memon, H. Zhuo, M. Zhao, Experimental study on CO_2 capture mechanisms using Na_2ZrO_3 sorbents synthesized by soft chemistry method, Chem. Eng. J. 313 (2017) 646-654.
[56] R.N. Kust, J.D. Burke, Thermal decomposition in alkali metal nitrate melts, Inorg. Nucl. Chem. Lett. 6 (1970) 333–335.
[57] H. Tsuji, T. Shishido, A. Okamura, Y. Gao, H. Hattori, H. Kita, Oxygen exchange between magnesium oxide surface and carbon dioxide, J. Chem. Soc., Faraday Trans. 90 (1994) 803-807.
[58] B. Liu, P.S. Thomas, A.S. Ray, J.P. Guerbois, ATG analysis of the effect of calcination conditions on the properties of reactivemagnesia, J. Therm. Anal. Calorim. 88 (2007) 145-149.

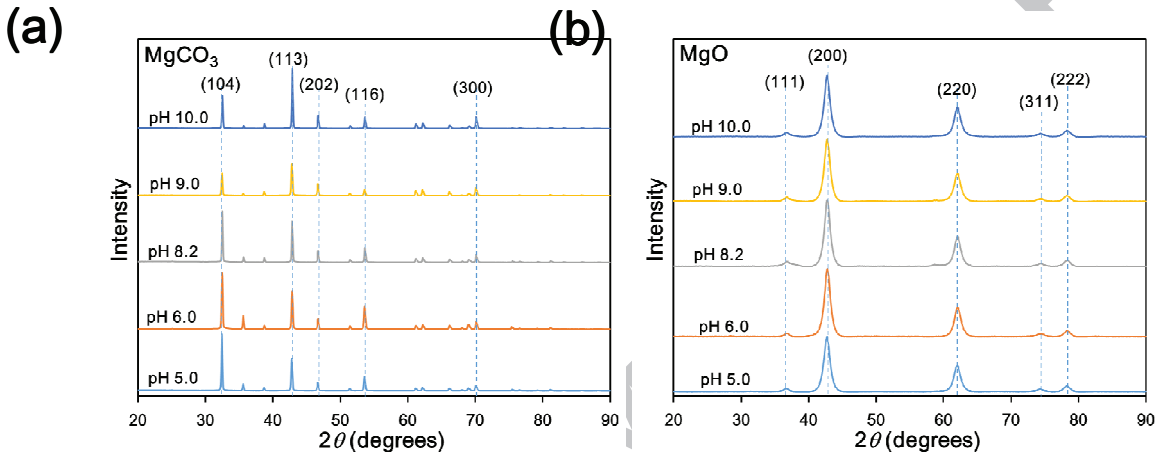

Fig. 1. Powder XRD patterns of (a) $MgCO_3$ synthesized at hydrothermal solution pH 5.0-10.0 and (b) MgO samples after annealing

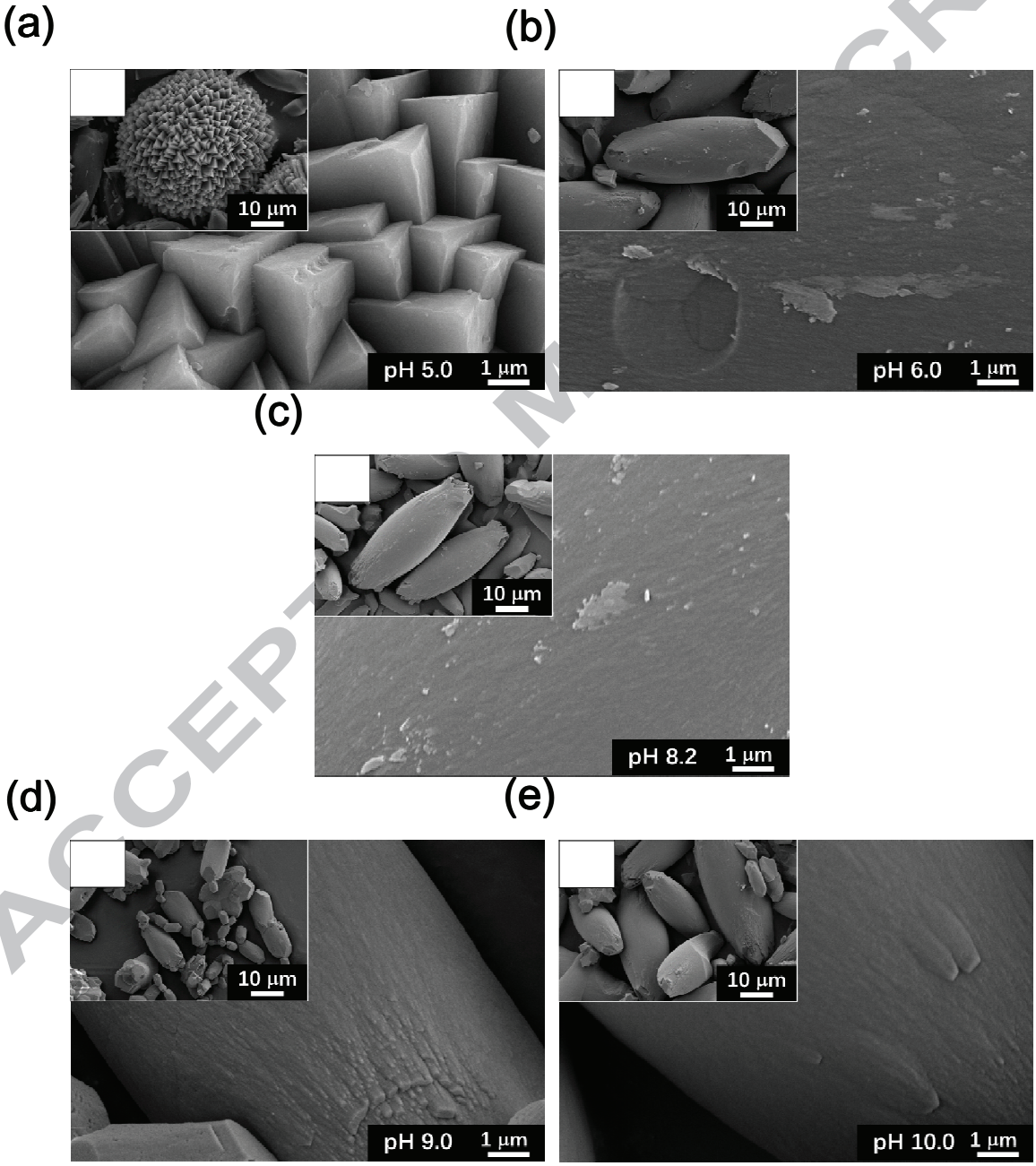

Fig. 2. SEM images of MgO synthesized at hydrothermal solution pH of (a) 5.0, (b) 6.0, (c) 8.2, (d) 9.0 and (e) 10.0.

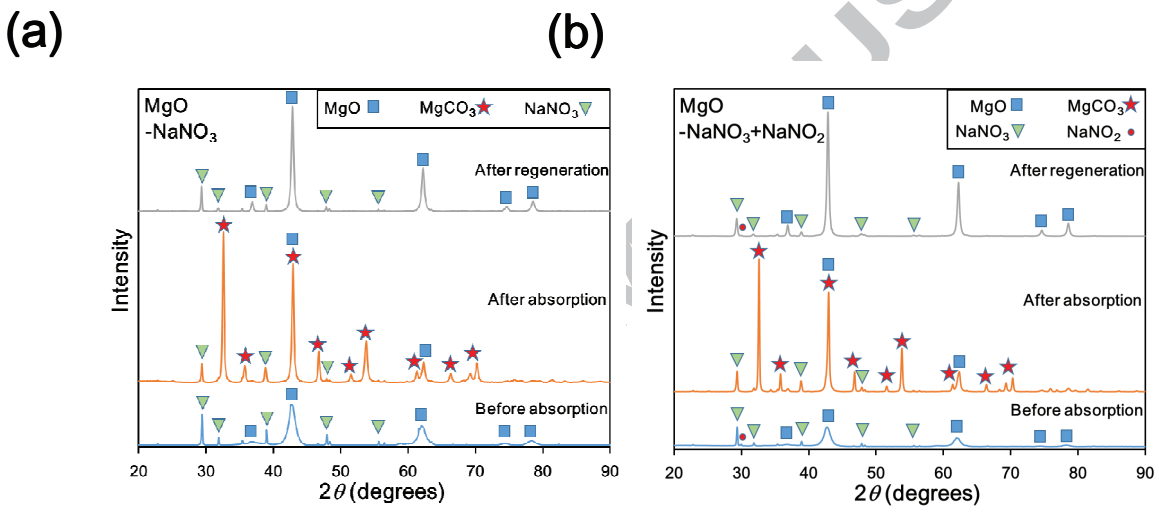

Fig. 3. Powder XRD patterns of (a) MgO-pH9.0 promoted with $NaNO_3$ and (b) MgO-pH9.0 promoted with $NaNO_3$+$NaNO_2$.

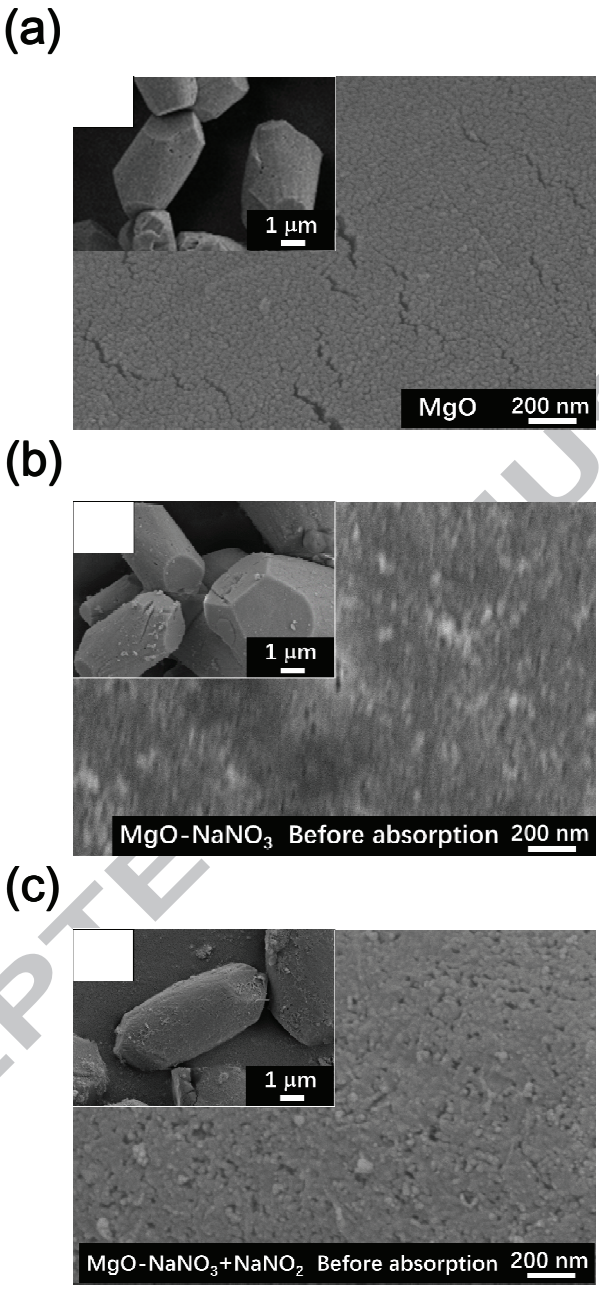

Fig. 4. SEM images of (a) MgO-pH9.0, (b) MgO promoted with $NaNO_3$, and (c) MgO promoted with $NaNO_3$+$NaNO_2$.

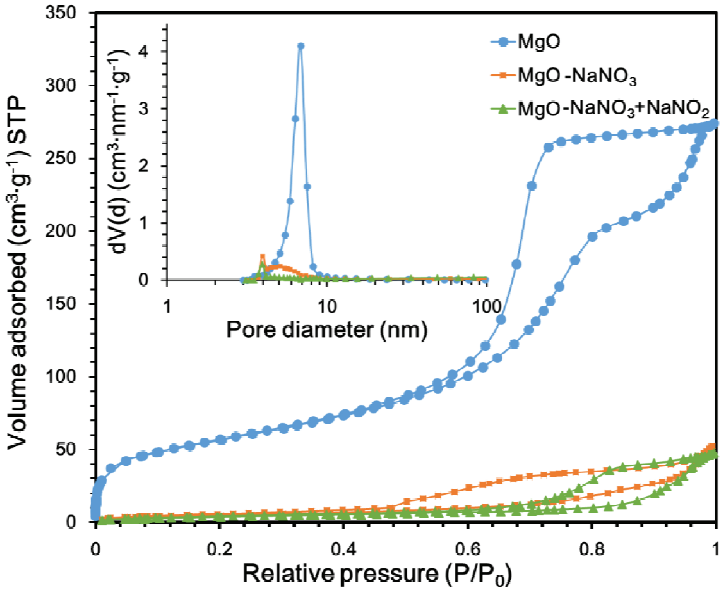

Fig. 5. N_2 adsorption/desorption isotherms of mesoporous MgO-pH9.0, MgO promoted with $NaNO_3$, and MgO promoted with $NaNO_3$+$NaNO_2$ (inset: BJH method pore size distribution for these three materials)

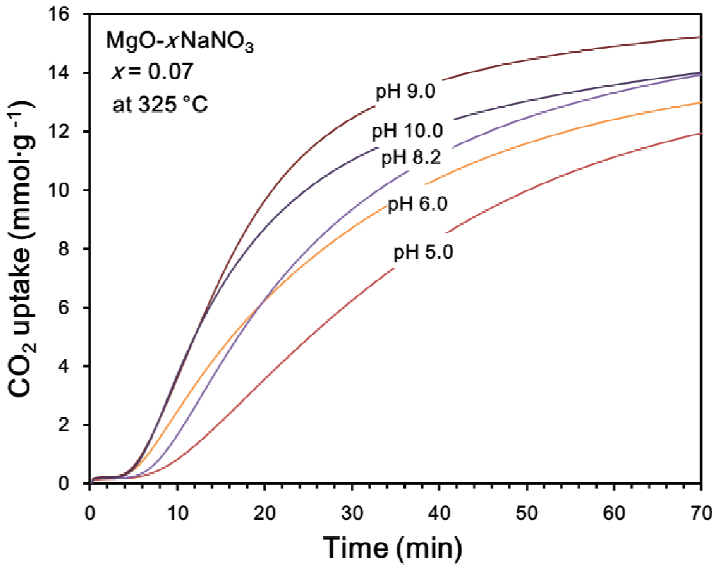

Fig. 6. CO_2 uptake by MgO synthesized at different solution pH. (Experimental conditions: 0.85 bar of CO_2, at temperature of 325 °C, $NaNO_3$ dose: x=0.07)

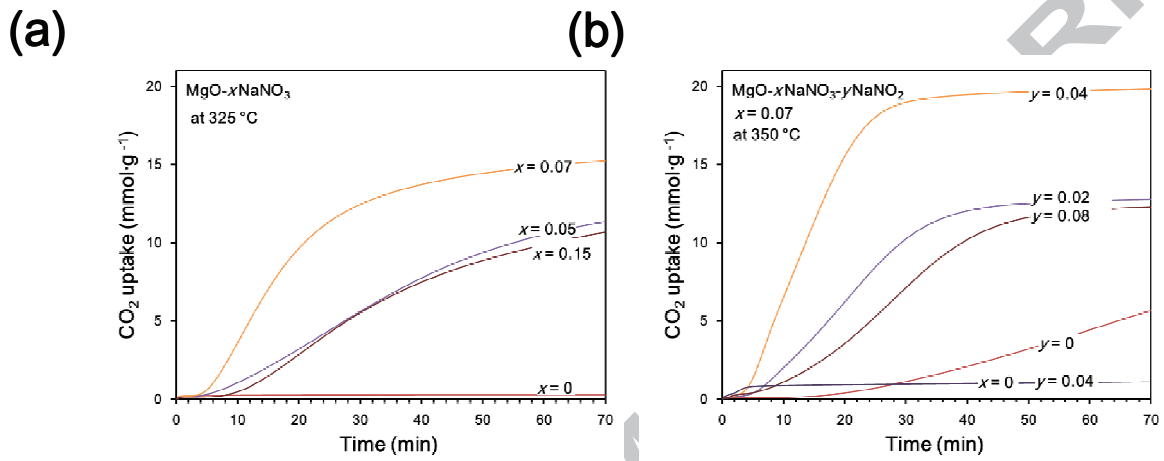

Fig. 7. CO_2 uptake by MgO-pH9.0 promoted by (a) $NaNO_3$ and (b) $NaNO_3$+$NaNO_2$. (Experimental conditions: 0.85 bar of CO_2, at temperature of 325 °C for Mg-$NaNO_3$ and 350 °C for Mg-$NaNO_3$+$NaNO_2$, MgO/$NaNO_3$/$NaNO_2$ molar ratio of 1:*x*:*y*)

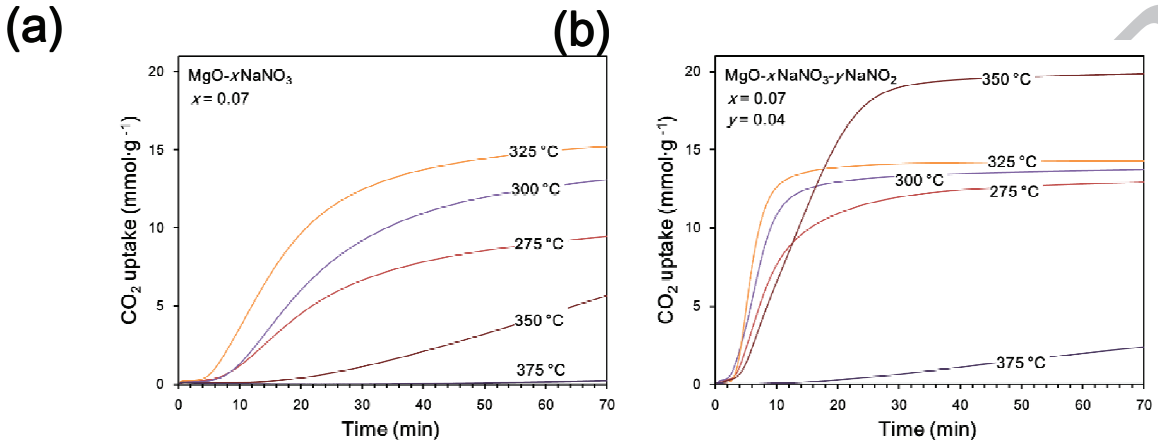

Fig. 8. CO_2 uptake by MgO-pH9.0 promoted by (a) $NaNO_3$ and (b) $NaNO_3$+$NaNO_2$ at temperature 275-375 °C. (Experimental conditions: 0.85 bar of CO_2, MgO/$NaNO_3$/$NaNO_2$ molar ratio of 1:*x*:*y*, *x*=0.07 and *y*=0.04)

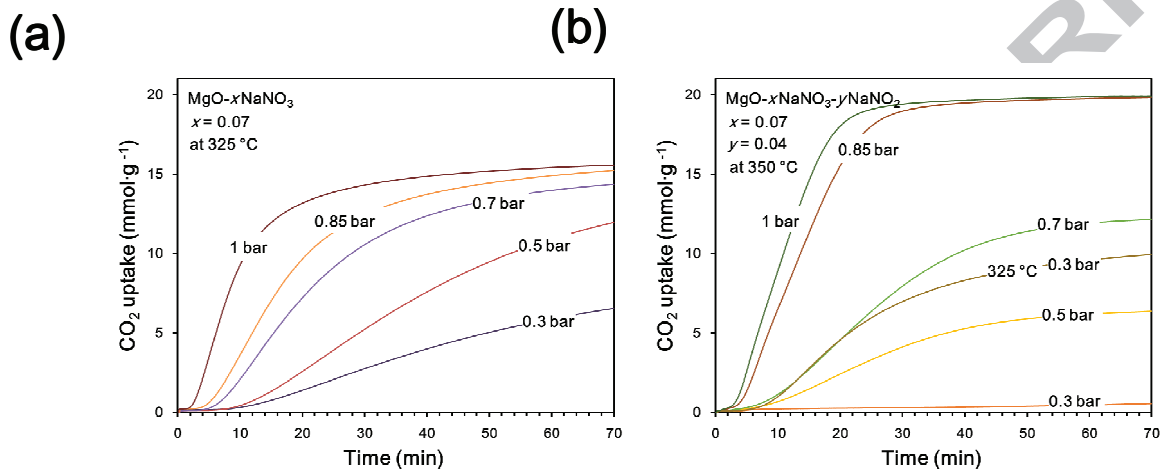

Fig. 9. CO_2 uptake by MgO-pH9.0 promoted by (a) $NaNO_3$ and (b) $NaNO_3$+$NaNO_2$ at different concentrations of CO_2. (Experimental conditions: at temperature of 325 °C for Mg-$NaNO_3$ and 350 °C for Mg-$NaNO_3$-$NaNO_2$, MgO/$NaNO_3$/$NaNO_2$ molar ratio of 1:*x*:*y*, *x*=0.07 and *y*=0.04)

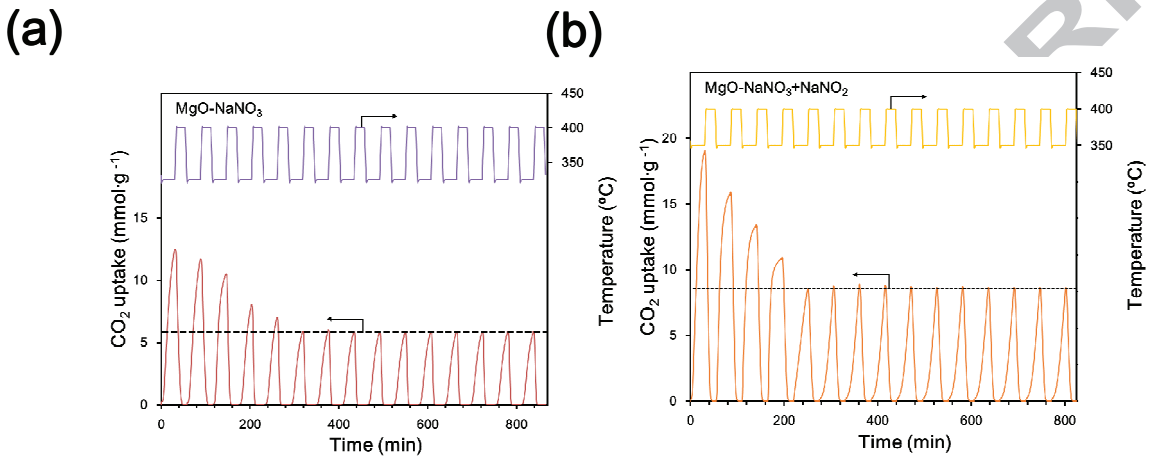

Fig. 10. CO_2 uptake over repeated cycles by MgO-pH9.0 promoted by (a) $NaNO_3$ and (b) $NaNO_3$+$NaNO_2$. (Experimental conditions: absorption temperature of 325 °C for Mg-$NaNO_3$ and 350 °C for Mg-$NaNO_3$-$NaNO_2$, 0.85 bar of CO_2 and absorption time of 30 min; desorption temperature of 400 °C for both materials in 1 bar of N_2 for 20 min)

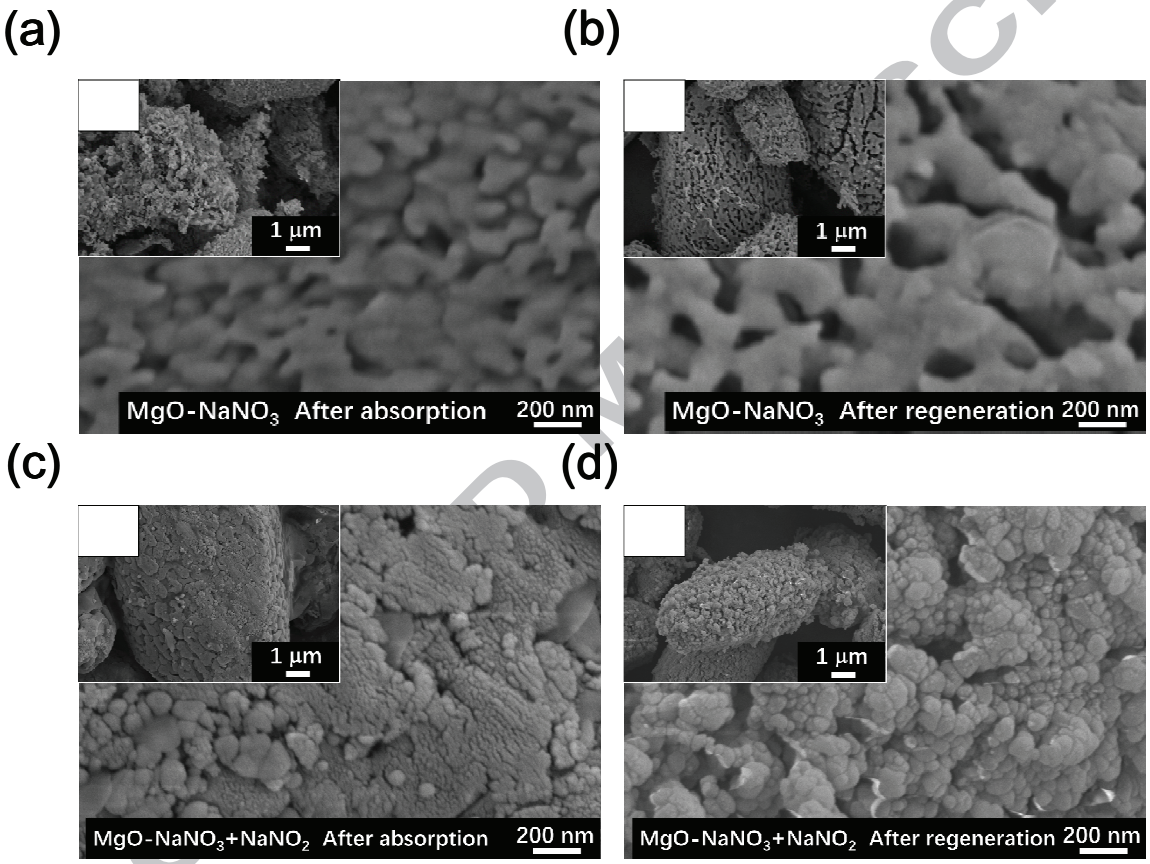

Fig. 11. SEM images of MgO-pH9.0 promoted with $NaNO_3$ (a) after absorption and (b) after regeneration (at the 15th cycle); MgO-pH9.0 promoted with $NaNO_3$+$NaNO_2$ (c) after absorption and (d) after regeneration (at the 15th cycle).

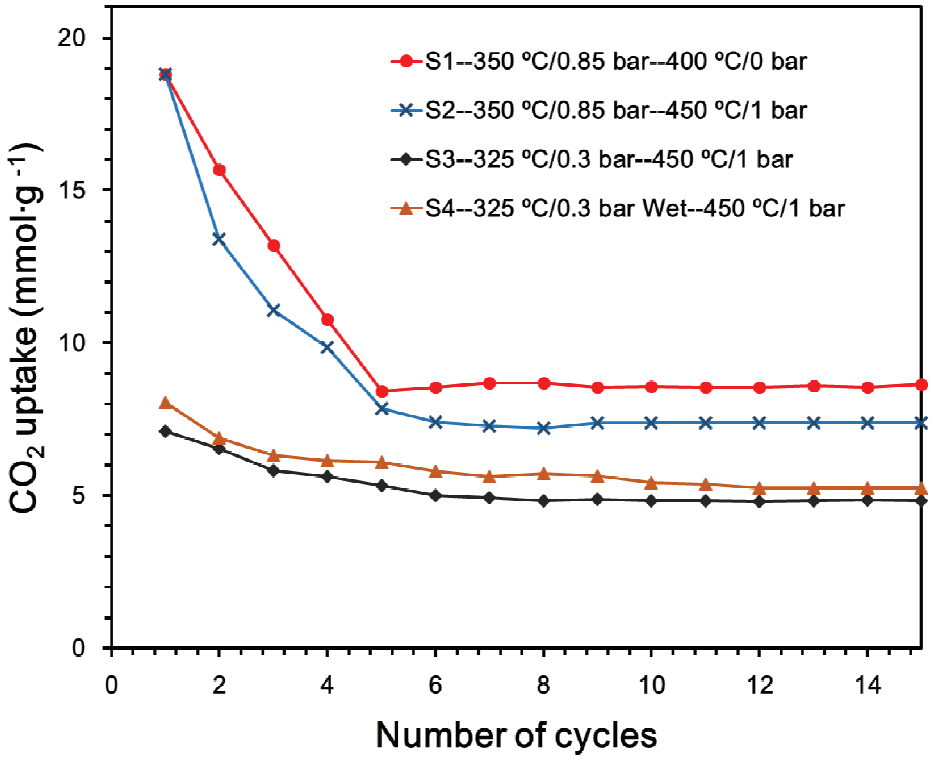

Fig. 12. CO_2 uptake over repeated cycles by MgO-pH9.0 promoted $NaNO_3$+$NaNO_2$. (Experimental conditions: For all scenarios, the carbonation and decarbonation time are 30 and 20 min, respectively. The carbonation and decarbonation conditions (temperature/partial pressure of CO_2) are: S1: Carbonated at 350 °C/0.85 bar and decarbonated at 450 °C/0 bar; S2: Carbonated at 350 °C/0.85 bar and decarbonated at 450 °C/1 bar; S3: Carbonated at 325 °C/0.3 bar and decarbonated at 450 °C/1 bar; S4: Carbonated at 325 °C/0.3 bar (with ~0.01 bar of steam) and decarbonated at 450 °C/1 bar.

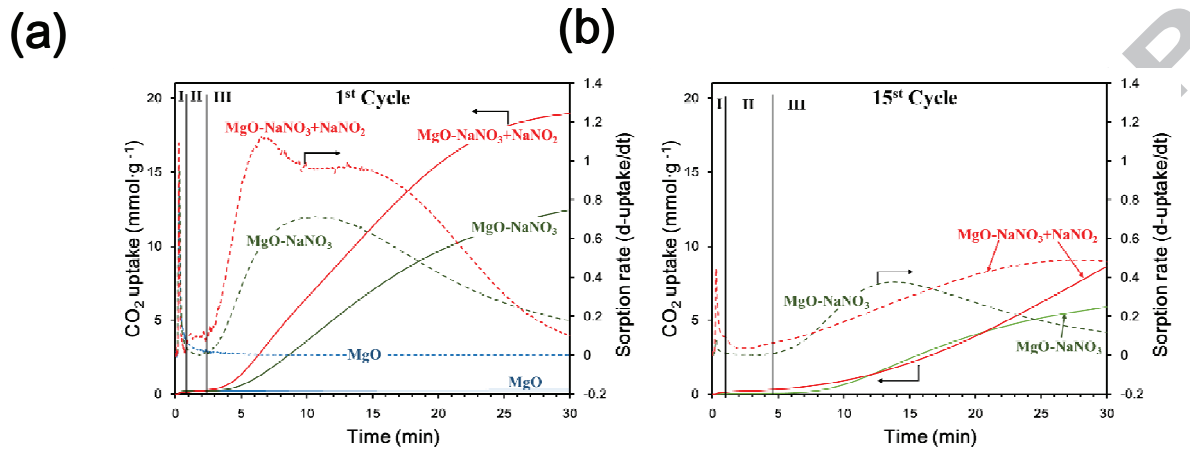

Fig. 13. CO_2 sorption kinetics with MgO or promoted MgO-pH9.0 at the (a) 1st cycle and (b) 15th cycle. (Solid line-primary axis: sorption data; Dashed line-secondary axis: sorption rate by the first order derivative)

Table 1. Crystallite size and textural properties of the MgO materials.

Sample	Crystallite size (nm)			BET surface area ($m^2 \cdot g^{-1}$)	Pore volume ($cm^3 \cdot g^{-1}$)	BJH average pore size (nm)
	(111)	(200)	(220)			
MgO-pH5.0	11.6	8.5	9.0	186	0.39	6.86
MgO-pH6.0	9.4	8.3	8.8	192	0.43	6.31
MgO-pH8.2	6.9	8.2	8.8	208	0.45	5.96
MgO-pH9.0	6.3	8.2	8.6	230	0.49	5.65
MgO-pH10.0	7.6	8.6	9.0	224	0.46	5.77
MgO-$NaNO_3$-before absorption	7.2	8.3	8.7	29	0.082	3.94
MgO-$NaNO_3$-after regeneration	27.7	21.7	21.2	20	0.026	3.28
MgO-$NaNO_3$+$NaNO_2$-before absorption	7.2	8.4	8.6	23	0.073	3.87
MgO-$NaNO_3$+$NaNO_2$-after regeneration	30.8	25.6	25.8	18	0.032	3.33

- Mesoporous MgO with different morphologies can be synthesized through hydrothermal method.
- Double promoters ($NaNO_3$/$NaNO_2$) enhance CO_2 capture kinetics and capacity of MgO.
- The interactions between the promoted MgO and CO_2 experience a “three stage” process.

Morphology control of MgO by varying hydrothermal pH